Prostate Cancer and Prostatic Disease (2015) 18, 128–136

www.nature.com/pcan

ORIGINAL ARTICLE

# Multiparametric MRI for detection of radiorecurrent prostate cancer: added value of apparent diffusion coefficient maps and dynamic contrast-enhanced images

M Abd-Alazeez[1,2], N Ramachandran[3], N Dikaios[3,4], HU Ahmed[1,5], M Emberton[1,5], A Kirkham[3], M Arya[1,6], S Taylor[3,4], S Halligan[3,4] and S Punwani[3,4]

**BACKGROUND:** Multiparametric magnetic resonance imaging (mp-MRI) is increasingly advocated for prostate cancer detection. There are limited reports of its use in the setting of radiorecurrent disease. Our aim was to assess mp-MRI for detection of radiorecurrent prostate cancer and examine the added value of its functional sequences.

**METHODS:** Thirty-seven men with mean age of 69.7 (interquartile range, 66–74) with biochemical failure after external beam radiotherapy underwent mp-MRI (T2-weighted, high *b*-value, multi-*b*-value apparent diffusion coefficient (ADC) and dynamic contrast-enhanced (DCE) imaging); then transperineal systematic template prostate mapping (TPM) biopsy. Using a locked sequential read paradigm (with the sequence order above), two experienced radiologists independently reported mp-MRI studies using score 1–5. Radiologist scores were matched with TPM histopathology at the hemigland level ($n = 74$). Accuracy statistics were derived for each reader. Interobserver agreement was evaluated using kappa statistics.

**RESULTS:** Receiver–operator characteristic area under curve (AUC) for readers 1 and 2 increased from 0.67 (95% confidence interval (CI), 0.55–0.80) to 0.80 (95% CI, 0.69–0.91) and from 0.67 (95% CI, 0.55–0.80) to 0.84 (95% CI, 0.76–0.93), respectively, between T2-weighted imaging alone and full mp-MRI reads. Addition of ADC maps and DCE imaging to the examination did not significantly improve AUC for either reader ($P = 0.08$ and 0.47 after adding ADC, $P = 0.90$ and 0.27 after adding DCE imaging) compared with T2+high *b*-value review. Inter-reader agreement increased from $k = 0.39$ to $k = 0.65$ between T2 and full mp-MRI review.

**CONCLUSIONS:** mp-MRI can detect radiorecurrent prostate cancer. The optimal examination included T2-weighted imaging and high *b*-value DWI; adding ADC maps and DCE imaging did not significantly improve the diagnostic accuracy.

*Prostate Cancer and Prostatic Disease* (2015) **18,** 128–136; doi:10.1038/pcan.2014.55; published online 3 February 2015

## INTRODUCTION

Men who undergo radiotherapy for localized prostate cancer have a one in three to one in four chance of biochemical failure at 5–8 years follow-up.[1] Biochemical failure is defined as either a PSA increase of $\geqslant 2\,\mathrm{ng\,dl^{-1}}$ above the nadir (phoenix definition)[2] or more than two consecutive rises of PSA above the nadir.[3] Fifteen percent of low-risk and 67% of high-risk prostate cancer patients biochemically relapse within 5 years of radiotherapy.[4] Yet the biochemical relapse does not always signify disease relapse and false-positive rates are reported as high as 32%.[4,5] Moreover, PSA elevation can represent recurrence of local disease or development of metastases. Therefore, stratification of patients between no therapy, salvage local therapy and systemic therapy remains to be a cause of concern.[6]

Conventional anatomical magnetic resonance imaging (MRI) using T2-weighted imaging has been evaluated for detection of local disease in this setting.[7] However, glandular atrophy and fibrosis induced by radiation therapy severely limit the accuracy. Several studies have demonstrated that microstructural and functional MRI techniques such as diffusion-weighted imaging (DWI) and dynamic contrast-enhanced (DCE) imaging, either performed individually[1,8–11] or as part of a multiparametric (mp) examination,[12–14] can improve the detection of recurrent disease following the radiotherapy. However, the robustness of studies that use transrectal ultrasound-guided biopsy as a reference standard to evaluate MRI[8,11–13,15] is limited, given the imperfections in the reference standard itself, that is, rates of false-negative findings on transrectal ultrasound-guided biopsy can be as high as 42%.[16]

Alternative and more robust reference standards are often difficult to obtain in the setting of potential radiorecurrent disease. Salvage radical prostatectomy is technically challenging and rarely performed. This means that 90% or more men who have radiorecurrent disease go onto androgen deprivation therapy and whole mount prostatectomy specimens are not readily available for direct correlation with MRI in this setting.[12,13,15,17–19] Even if they are, it is likely that large selection biases will exist and limit external validity to the biochemical failure group.

Template prostate mapping (TPM) provides an alternative to systematic biopsy. It can sample the entire gland. We have previously reported the outcomes of MRI versus TPM biopsies in a single-center study of 13 patients.[18] Furthermore, there is little described on precisely which MRI sequences are necessary for the best diagnostic performance for detection of radiorecurrent

[1]Department of Urology, University College Hospital NHS Foundation Trust, London, UK; [2]Department of Urology, Faculty of Medicine, Fayoum University, Fayoum, Egypt; [3]Department of Radiology, University College London Hospital, London, UK; [4]Centre for Medical Imaging, University College London, London, UK; [5]Division of Surgery and Interventional Science, University College London, London, UK and [6]Barts Cancer Institute, Queen Mary University of London, London, UK. Correspondence: Dr M Abd-Alazeez, Division of Surgery and Interventional Science, University College London, 67-73 Riding House Street, London W1W 7EJ, UK.
E-mail: mohamed.azeez.10@ucl.ac.uk
Received 16 October 2014; revised 16 November 2014; accepted 10 December 2014; published online 3 February 2015

**Table 1.** 1.5-T Siemens MRI scan parameters

| | *TR (ms)* | *TE (ms)* | *Flip angle (degree)* | *Slice orientation* | *Slice thickness (mm)* | *FOV (mm)* | b-*value* ($s\,mm^{-2}$) | *NEX* | *Acquisition time (min:sec)* |
|---|---|---|---|---|---|---|---|---|---|
| T2 TSE | 5170 | 92 | 180 | Axial/coronal | 3/3 | 180 × 180/180 × 180 | n/a | 2 | 3:54/4:18 |
| STIR-EPIDWI (multi-*b* with ADC map) | 2200 | 98 | 90 | Axial | 5 | 260 × 260 | 0,150, 500,1000 | 16 | 5:44 |
| STIR-EPIDWI (high *b*) | 2200 | 98 | 90 | Axial | 5 | 320 × 320 | 1400 | 32 | 3:39 |
| 3D GRE | 5.61 | 2.52 | 15 | Axial | 3 | 260 × 260 | n/a | 1 | 7:00 (17 s/acquisition) |

Abbreviations: ADC, apparent diffusion coefficient; DWI, diffusion-weighted imaging; FOV, field of view; GRE, gradient echo; NEX, number of averages; STIR-EPI, short-tau inversion recovery echo planar imaging; TE, echo time; TR, repetition time; TSE, turbo spin time.

**Table 2.** 3 T Philips MRI scan parameters

| | *TR (ms)* | *TE (ms)* | *Flip angle (degree)* | *Slice orientation* | *Slice thickness* | *FOV (mm)* | b *value* ($s\,mm^{-2}$) | *NEX* | *Acquisition time (min:sec)* |
|---|---|---|---|---|---|---|---|---|---|
| T2 TSE | 7340 | 101 | 150 | Axial, coronal | 3 (10% gap) | 200 × 200 | n/a | 2 | 5:00/ 5:20 |
| STIR-EPI (multi-*b* with ADC map) | 4300 | 80 | 90 | Axial | 5 | 25 × 21 | 0,150, 500,1000 | 6 | 5:58 |
| STIR-EPI (high *b*) | 7500 | 79 | 90 | Axial | 5 | 25 × 21 | 2000 | 6 | 5:34 |
| 3D GRE | 17.07 | 3.62 | 15 | Axial | 3 | 256 × 256 | n/a | 2 | 2:72 (13 s/acquisition) |

Abbreviations: ADC, apparent diffusion coefficient; DWI, diffusion-weighted imaging; FOV, field of view; GRE, gradient echo; NEX, number of averages; STIR-EPI, short-tau inversion recovery echo planar imaging; TE, echo time; TR, repetition time; TSE, turbo spin time.

disease.[15,17] Our aim was to evaluate the diagnostic accuracy of mp-MRI in a larger cohort of men and explore the added diagnostic value of functional sequences (DWI and DCE imaging) for the detection of radiorecurrent disease using TPM biopsy as the reference standard.

## MATERIALS AND METHODS

The institutional review board approved the re-evaluation of patient data sets acquired for other research studies or during the routine clinical care (R&D No: 12/0195, date 16 July 2012).

### Patient population

Our institutional TPM biopsy database of 509 patients was interrogated to identify patients presenting with biochemical failure following radiotherapy and who had undergone: (a) subsequent standardized mp-MRI (T2-weighted imaging, DWI (high *b*-value and apparent diffusion coefficient (ADC) map) and DCE imaging) and (b) TPM biopsy. The updated definition of biochemical recurrence as stated by Phoenix was used.[2]

Out of 49 patients eligible for inclusion; (a) five were excluded owing to history of brachytherapy; (b) one was excluded owing to limited TPM biopsy sampling, that is, less than 20 cores or non-systematic zonal sampling and (c) six were excluded owing to incomplete MRI arising from hip prosthesis artifact. This left a final study cohort of 37.

### MRI protocol

Imaging was performed on two separate platforms, either 1.5 T (Siemens Avanto, $n = 34$) (Siemens Healthcare, Erlangen, Germany) or 3.0 T (Philips Achieva, $n = 3$) (Philips Healthecare, Best, Netherlands). In each case the manufacturers' multichannel, only pelvic phased array coil was used for imaging. MRI comprised of T2-weighted imaging, DWI and DCE imaging. DWI consisted of multiple *b*-values, the highest *b*-value was $b = 1400\ s\text{-}mm^{-2}$ at 1.5T and $b = 2000\ s\,mm^{-2}$ at 3.0 T.

Twenty milligrams of buscopan was administered intravenously before acquisition. Initially, T2-weighted images were acquired, followed by DWI and finally DCE imaging. For DCE imaging, 0.1 mmol $kg^{-1}$ megluminegadoterate (Dotarem, Guerbet, Villepinte, France) was administered at 3 ml $s^{-1}$ followed by 10 ml of saline chaser and T1-weighted imaging repeated through the gland volume with a temporal resolution of 13 s at 3 T and 17 s at 1.5 T. Full sequence parameters for 1.5-T and 3.0-T scans are given in Tables 1 and 2.

**Table 3.** Patient demographics

| | *All patients (n = 37)* |
|---|---|
| Age (mean, IR) | 69.7 (66–74) |
| PSA at time of MRI (median, IR) | 4.5 (3–7.3) |
| Time between end of DXT and MRI (months) (median, IR) | 66 (54–90) |
| Time between MRI and biopsy (months) (median, IR) | 2 (1–3) |
| Total biopsy cores/patient (median, IR) | 41 (31–52) |
| Positive cores/patient (%) | 17 (9–30) |
| *Clinical stage at diagnosis* | |
| 1b | 1 |
| 1c | 8 |
| 2a | 7 |
| 2b | 1 |
| 2c | 4 |
| 3a | 10 |
| 3b | 6 |
| *Gleason score at diagnosis* | |
| 3+3 | 15 |
| 3+4 | 9 |
| 4+3 | 2 |
| 4+4 | 4 |
| 4+5 | 6 |
| 5+4 | 1 |
| *Hormones before MRI* | |
| Yes | 27 |
| No | 10 |

Abbreviation: DXT, deep x-ray therapy; IR, interquartile range; MRI, magnetic resonance imaging.

### Image viewing

Anonymous studies were independently reviewed on an OsiriX workstation (version 3.7.1 32-bit) (Pixmeo, Geneva, Switzerland) by two experienced radiologists (with 7 and 5 years of mp-MRI prostate experience).

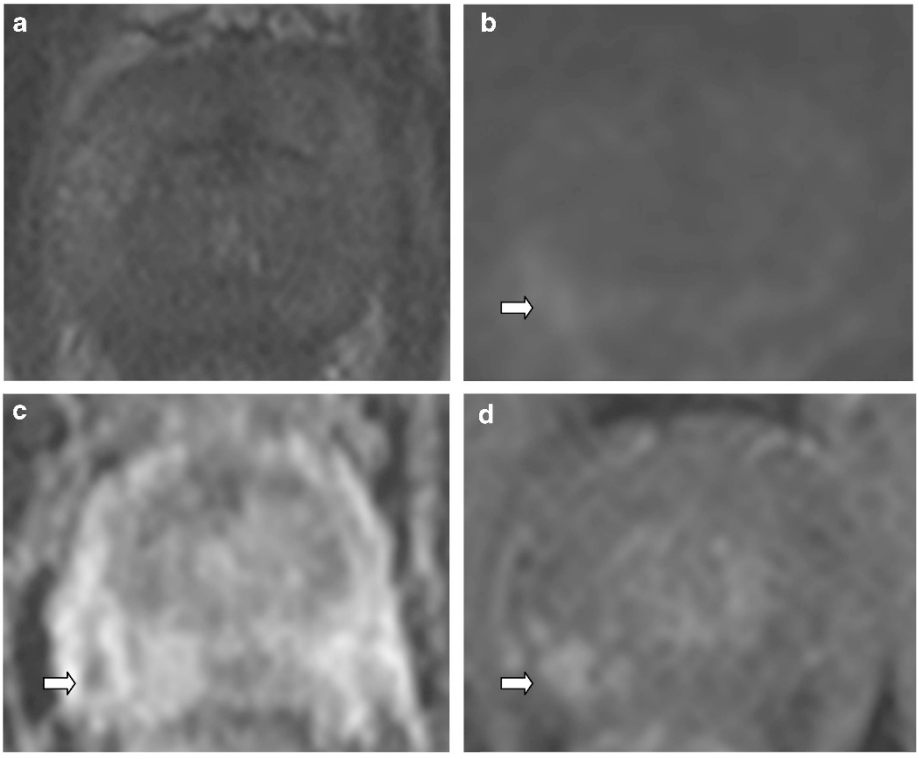


**Figure 1.** Axial images from a 68-year-old patient with positive MRI (scoring 5/5), nine positive cores with a maximum cancer core length of 6 mm, 50%, Gleason 3+4 were present at template prostate mapping (TPM) biopsy in the right lateral zone. Both the readers scored the right hemigland as: 3/5 on T2 weighted (**a**); 4/5 on b1400 (**b**); on apparent diffusion coefficient (ADC) (**c**); and 5/5 on dynamic contrast-enhanced (DCE) imaging (**d**). The left hemigland was scored by readers 1 and 2 as: 3/5 and 3/5 on T2 weighted (**a**); 2/5 and 2/5 on b1400 (**b**); 2/5 and 2/5 on ADC (**c**); and 2/5 and 1/5 on DCE (**d**). No cancer was present in the left hemigland on TPM biopsy.

Both the radiologists were aware of the history of radiotherapy and biochemical relapse; but were unaware of other clinical details, PSA value or histology. Both the radiologists performed a locked sequential read in a single session with the following read order:

1. T2-weighted images
2. T2-weighted+high *b*-value images
3. T2-weighted+high *b*-value+ADC images
4. T2-weighted+high *b*-value+ADC+DCE images

For each read, the radiologists scored the left and right hemiglands for likelihood of cancer using mp-MRI parameters as recently published by the European Society of Urogenital Radiology[20] and scored 1–5, where: 1 = highly unlikely cancer, 2 = unlikely cancer, 3 = equivocal, 4 = likely cancer and 5 = highly likely cancer.

### Transperineal TPM biopsy

Patients with biochemical failure following radiotherapy were routinely offered TPM biopsy at our institution. All patients within the study cohort underwent TPM biopsy under general anesthesia using a 5-mm sampling frame as in the method previously described by Barzell and Melamed.[21] In all the included patients the full gland was systematically sampled. The mean time from mp-MRI to TPM biopsy was 2.1 months (interquartile range, 1–3 months).

### Histopathology and mp-MRI matching

Pathologists were aware that the patients had biochemical failure after radiotherapy with or without neoadjuvant/adjuvant hormonal treatment at time of radiotherapy treatment. Only cores with no pronounced radiation/hormone effect were assigned a Gleason score. All the patients with positive TPM biopsy included in the study have been given Gleason scores. Primary and secondary Gleason patterns of tumor were recorded for each positive core, together with the cancer core length (length of cancer in each core excluding intervening normal areas).[22] Histopathology matching was based on the presence of any cancer regardless of the clinical significance. We also performed the analysis according to the presence of clinically significant disease using different mp-MRI thresholds in the Appendix. mp-MRI reader scores were matched to the histopathology at the hemigland level.

### Statistical analysis

Sensitivity, specificity, positive predictive values (PPV) and negative predictive values (NPV) together with positive and negative likelihood ratios ($LR^+$ and $LR^-$) were calculated for each reader at each locked sequential read step using MedCalc v13.0.0.0. (Medcalc, Ostend, Belgium) mp-MRI threshold of 3 was used to indicate positive recurrence of cancer. Receiver–operator characteristic (ROC) area under curve (AUC) analysis was performed for each reader at each locked sequential read step using SPSS v22 (IBM; Armonk, New York, USA) and the significant changes were statistically assessed as previously described[23] with MedCalc. McNemar's test was used to detect statistically significant differences between variable sensitivities and specificities of different mp-MRI data sets.

Interobserver agreement was evaluated using Cohen's Kappa coefficient statistics. To test the agreement, the 1–5 scores were categorized into three groups on the basis of clinical interpretation: negative (score 1 and 2); equivocal (score 3) and positive (score 4 and 5) for cancer. Kappa values of 0.00–0.20 were considered as 'slight'; 0.21–0.40, 'fair'; 0.41–0.60, 'moderate'; 0.61–0.80, 'substantial'; and 0.81–1.00, 'almost perfect' agreement.[24]

## RESULTS

Forty-nine out of seventy-four (66%) hemiglands (thirty-three patients) showed positive TPM biopsy. Table 3 shows baseline demographics of patients included in the study. A typical mp-MRI

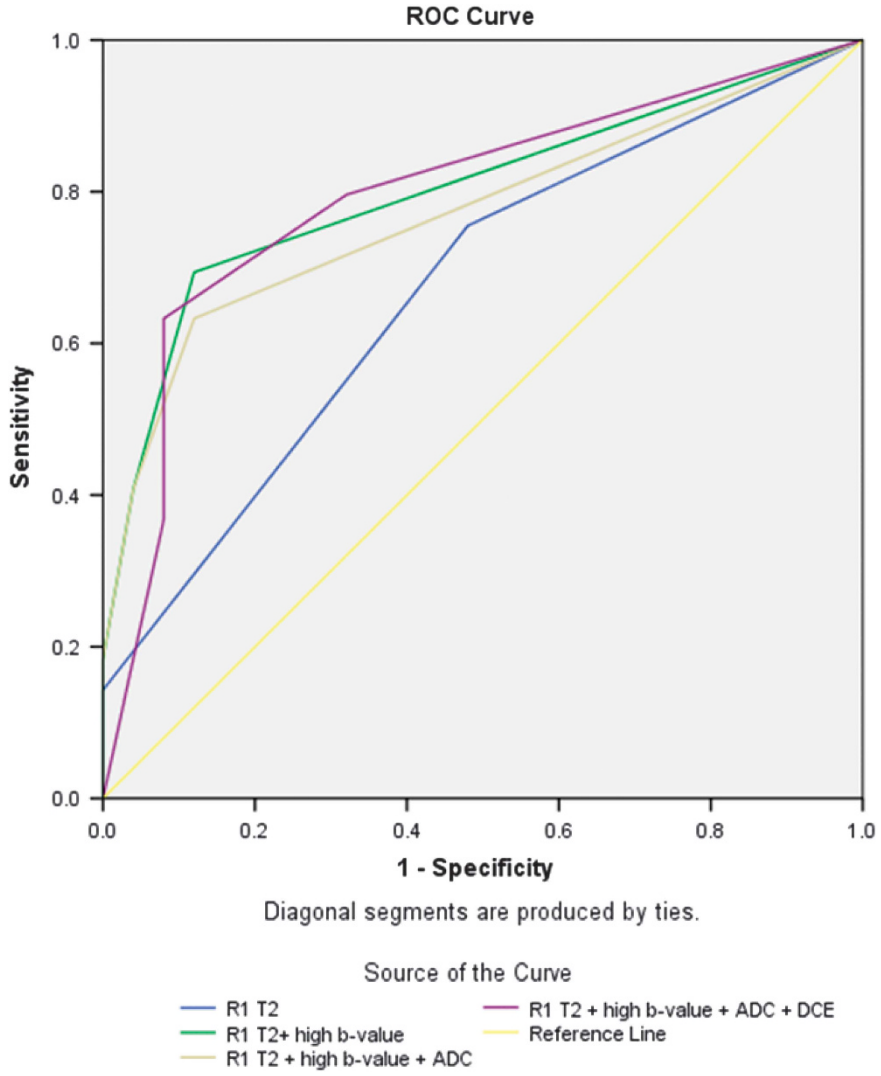


**Figure 2.** Receiver–operator characteristic (ROC) curves of reader 1 for the four locked sequential read. ROC-AUC for T2, T2+high *b*-value, T2+high *b*-value+apparent diffusion coefficient (ADC) and T2+high *b*-value+ADC+dynamic contrast-enhanced (DCE) imaging were 0.67, 0.80, 0.77 and 0.80, respectively.

data set for locked sequential read scores for readers 1 and 2 is presented in Figure 1.

Figures 2 and 3 show the ROC curves of AUC (ROC-AUC) for readers 1 and 2 at each locked sequential read step, respectively. Tables 4a and 4b show the accuracy figures (sensitivity, specificity, PPV, NPV, $LR^+$ and $LR^-$) for both the readers at different locked sequential read.

First-read: T2-weighted imaging

Sensitivity/specificity and PPV/NPV were 76%/52% and 76%/52%, respectively, for reader 1, and 78%/44% and 73%/50%, respectively, for reader 2.

The ROC-AUC, for classification of hemigland status, was 0.67 (95% CI 0.55–0.80) for both readers 1 and 2 (Table 5).

There was a 'fair' interobserver agreement ($\kappa = 0.39$; 95% CI 0.20–0.58) between the two readers (Table 6).

Second-read: T2-weighted+high *b*-value DWI

Sensitivity/specificity and PPV/NPV were 69%/88% and 92%/59%, respectively, for reader 1, and 65%/92% and 94%/58%, respectively, for reader 2.

With addition of high *b*-value DWI, the ROC-AUC significantly improved for both the readers to 0.80 (95% CI, 0.70–0.92 and 0.70–0.90 for readers 1 and 2, respectively) ($P = 0.02$ and 0.01 for readers 1 and 2, respectively).

Interobserver agreement was 'moderate' ($\kappa = 0.51$; 95% CI 0.36–0.64) following the review of high *b*-value DWI.

Third-read: T2-weighted+high *b*-value DWI+ADC maps

Sensitivity/specificity and PPV/NPV were 63%/88% and 91%/55%, respectively, for reader 1, and 63%/92% and 94%/56%, respectively, for reader 2.

There was no statistically significant change in ROC-AUC for either reader on additional review of ADC maps (ROC-AUC = 0.77, $P = 0.08$ for reader 1; ROC-AUC = 0.77, $P = 0.47$ for reader 2).

Interobserver agreement was moderate ($\kappa = 0.48$; 95% CI 0.31–0.64).

Final-read: T2-weighted+high *b*-value DWI+ADC maps+DCE imaging

Sensitivity/specificity and PPV/NPV were 80%/68% and 83%/63% respectively, for reader 1, and 76%/72% and 84%/60%, respectively, for reader 2.

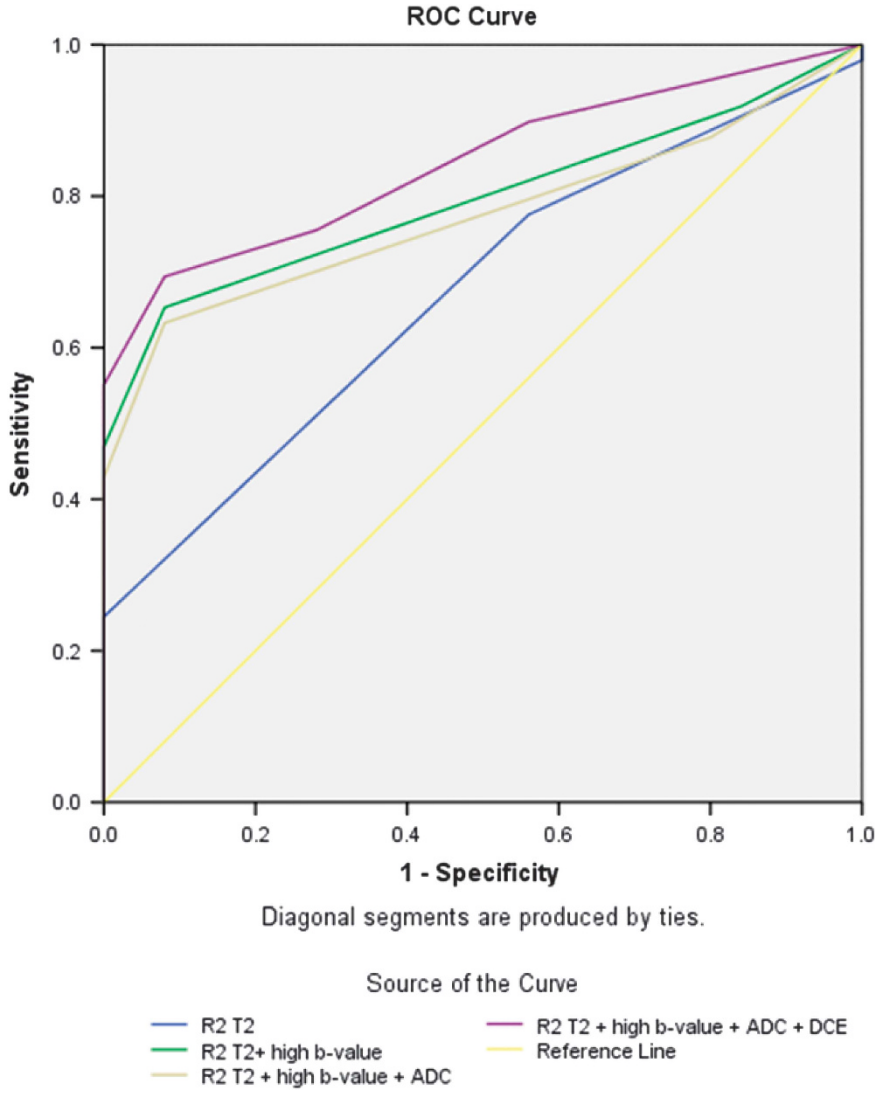


**Figure 3.** Receiver–operator characteristic (ROC) curves of reader 2 for the four locked sequential read. ROC-AUC for T2, T2+high b-value, T2+high b-value+apparent diffusion coefficient (ADC) and T2+high b-value+ADC+dynamic contrast-enhanced (DCE) imaging were 0.67, 0.80, 0.77 and 0.84, respectively.

ROC-AUC was marginally, but not significantly, higher after the inclusion of DCE images (0.80, 95% CI: 0.69–0.91 for reader 1 and 0.84, 95% CI: 0.76–0.93 for reader 2) compared with the T2+high *b*-value ($P=0.90$ and 0.27 for readers 1 and 2, respectively) and T2 +high *b*-value+ADC reads ($P=0.47$ and 0.11 for readers 1 and 2, respectively).

Interobserver agreement was 'substantial' ($\kappa=0.65$; 95%-CI 0.51–0.79).

### Comparison of diagnostic accuracy between locked sequential read steps

Sensitivity was highest for the full mp-MRI data set read (80% and 76% for readers 1 and 2, respectively). However, there was no statistically significant difference in sensitivity between full mp-MRI data set and T2+high *b*-value ($P=0.13$ and 0.23 for readers 1 and 2, respectively).

Specificity was highest at T2+high *b*-value and T2+high *b*-value +ADC (88% and 88% for reader 1 and 92% and 92% for reader 2, respectively). This was significantly higher than that of T2 alone ($P=0.004$ and $P=0.002$ for readers 1 and 2, respectively). There was no statistically significant difference on adding DCE imaging at the final read ($P=0.063$ for both the readers).

The highest $LR^+$ was 5.78 and 8.16 for readers 1 and 2 at the locked sequential read of T2+high *b*-value. This was higher than that for the T2-weighted imaging alone (1.57 and 1.38 for readers 1 and 2, respectively) and full mp-MRI data set (2.49 and 2.70 for readers 1 and 2, respectively).

## DISCUSSION

Although evidence is starting to emerge that mp-MRI can aid in the detection of local disease following radiotherapy, study sizes remain small and what constitutes an optimal mp-MRI data set remains unknown.[15,18] In this work, we explored the incremental value of individual mp-MRI sequences for the detection of radiorecurrent prostate cancer validated against a robust TPM biopsy reference. We employed a locked sequential read paradigm using T2-weighted imaging, high *b*-value DWI, ADC maps and DCE imaging. Our sequence of reading mp-MRI pictures in the current study was T2-weighted≫high *b*-value≫ADC maps then DCE imaging. Our cohort was homogenous, all our patients

**Table 4a.** Reader performance at the hemigland level with mp-MRI score ⩾3 as positive

| | *R1* | | | | *R2* | | | |
|---|---|---|---|---|---|---|---|---|
| | *T2W* | *T2W+high* b-*value* | *T2W+high* b-*value+ADC* | *T2W+high* b-*value+ ADC+DCE* | *T2W* | *T2W+high* b-*value* | *T2W+high* b-*value+ADC* | *T2W+high* b-*value+ADC+DCE* |
| Sensitivity | 76 | 69 | 63 | 80 | 78 | 65 | 63 | 76 |
| Specificity | 52 | 88 | 88 | 68 | 44 | 92 | 92 | 72 |
| PPV | 76 | 92 | 91 | 83 | 73 | 94 | 94 | 84 |
| NPV | 52 | 59 | 55 | 63 | 50 | 58 | 56 | 60 |
| $LR^+$ | 1.57 | 5.78 | 5.27 | 2.49 | 1.38 | 8.16 | 7.91 | 2.7 |
| $LR^-$ | 0.47 | 0.35 | 0.42 | 0.3 | 0.51 | 0.38 | 0.4 | 0.34 |

Abbreviations: ADC, apparent diffusion coefficient; DCE, dynamic contrast-enhanced imaging; $LR^+$, positive likelihood ratios; $LR^-$, negative likelihood ratios; NPV, negative predictive values; PPV, positive predictive values; R1, reader 1; R2, reader 2; T2W, T2 weighted.

**Table 4b.** *P*-values between different mp-MRI reads at threshold ⩾3 as positive

| | *R1* | | *R2* | |
|---|---|---|---|---|
| | *Sensitivity* | *Specificity* | *Sensitivity* | *Specificity* |
| T2 vs T2+high *b*-value | 0.548 | 0.004 | 0.146 | 0.002 |
| T2 vs T2+high *b*-value+ ADC | 0.179 | 0.004 | 0.065 | 0.002 |
| T2 vs T2+high *b*-value+ ADC+DCE | 0.791 | 0.388 | 1.0 | 0.923 |
| T2+high b-value vs T2+ high *b*-value+ADC+DCE | 0.125 | 0.063 | 0.227 | 0.063 |

Abbreviations: ADC, apparent diffusion coefficient; DCE, dynamic contrast-enhanced imaging; R1, reader 1; R2, reader 2.

**Table 6.** Interobserver agreement between readers of locked sequential mp-MRI reads

| | *Interobserver agreement* | | | |
|---|---|---|---|---|
| | *T2W* | *T2W+high* b-*value* | *T2W+high* b-*value+ADC* | *T2W+high* b-*value+ ADC+DCE* |
| $\kappa$ | 0.392 | 0.512 | 0.475 | 0.648 |
| SE | 0.097 | 0.08 | 0.084 | 0.073 |
| 95% CI | 0.202–0.581 | 0.356–0.699 | 0.309–0.640 | 0.505–0.791 |
| Wt $\kappa$ | 0.468 | 0.632 | 0.596 | 0.722 |
| Agreement | Fair | Moderate | Moderate | Substantial |

Abbreviations: ADC, apparent diffusion coefficient; DCE, dynamic contrast-enhanced imaging; SE, standard error; Wt $\kappa$ , weighted kappa.

**Table 5.** Receiver–operator characteristic area under curve (ROC-AUC)

| | *Area* | *Std.* | *95% Confidence interval* | |
|---|---|---|---|---|
| | | | *Lower bound* | *Upper bound* |
| *(a) Reader 1* | | | | |
| T2 | 0.67 | 0.065 | 0.55 | 0.80 |
| T2, b1400 | 0.80 | 0.051 | 0.70 | 0.92 |
| T2, high *b*-value, ADC | 0.77 | 0.054 | 0.67 | 0.88 |
| T2, high *b*-value, ADC, DCE | 0.80 | 0.055 | 0.69 | 0.91 |
| *(b) Reader 2* | | | | |
| T2 | 0.67 | 0.063 | 0.55 | 0.80 |
| T2, high *b*-value | 0.80 | 0.051 | 0.70 | 0.90 |
| T2, high *b*-value, ADC | 0.77 | 0.053 | 0.67 | 0.88 |
| T2, high *b*-value, ADC, DCE | 0.84 | 0.044 | 0.76 | 0.93 |

Abbreviations: ADC, apparent diffusion coefficient; DCE, dynamic contrast-enhanced imaging; Std., standard of error.

had previous external beam radiotherapy only and we did not include patients with brachytherapy as in other studies.[13,15]

Consistent with the work of others, our results show that addition of 'functional' MRI sequences to the anatomical T2-weighted imaging improves the performance of readers detecting radiorecurrent prostate cancer.[13,18,19] However, we did not observe a statistically significant increase in ROC-AUC of readers between T2-weighted imaging+high *b*-value DWI and sequential addition of ADC and DCE MRI.

A single preliminary study of mp-MRI (validated by TPM biopsy) suggested a good performance for detection of radiorecurrent prostate cancer.[18] AUC of the ROC curves for the two readers were reported as 0.77 and 0.89 for all the cancers and 0.86 and 0.93 for cancer core lengths ⩾3 mm (clinically significant). Our results of a larger cohort are in line with that previous study. Moreover, in the current study we looked at the added value of functional MRI sequences to the basic anatomical T2-weighted sequence. Akin *et al.*[13] have also reported on mp-MRI performance in the radiorecurrent setting. Analysis was performed at patient and prostate sextant levels where transrectal ultrasound-guided biopsy (12–16 cores) was used as the reference standard. They did not perform a locked sequential read for each sequence. Yet, our results on the overall performance of mp-MRI are in agreement with their work.

Recent work shows that DWI, either using ADC and/or high *b*-value, has similar sensitivity and higher specificity compared with DCE imaging in patients with radiorecurrent prostate cancer.[8,10,19,25] There is little data on the incremental value of DCE imaging to other mp-MRI sequences for radiorecurrent disease. Donati *et al.*[15] showed that DCE imaging did not add significant value in such patients. Our study compared the utility of high *b*-value DWI in combination with multi-*b*-value DWI-derived ADC maps, an area that was not covered by the work of Donati *et al.* We found no significant incremental value of reading ADC after high *b*-value DWI ($P = 0.08$ and 0.47 for readers 1 and 2, respectively) and in keeping with their work the subsequent addition of DCE imaging. It is likely that DCE images do add value

when used exclusively in conjunction with T2 imaging; Haider *et al.*[11] found better performance of DCE imaging than T2-weighted imaging in localization of prostate cancer. However, no DWI was included in their study. Kim *et al.*[17] found no statistically significant difference in sensitivity/specificity or accuracy among DWI, DCE imaging and both the sequences combined. However, they found statistically significant difference in ROC-AUC between combined DCE imaging+DWI and each isolated sequence.

Our inter-reader agreement data also demonstrate that agreement between readers improved with the addition of 'functional' imaging ($\kappa = 0.65$, 95% CI 0.51–0.79), which is comparable to other studies.[13,18] The lowest agreement was for T2 ($\kappa = 0.39$, 95% CI 0.20–0.58), which is also comparable to that in the literature.[13] Our results confirm that, should a patient be considered for salvage treatment after biochemical recurrence, T2-weighted together with high *b*-value DWI are the minimum needed sequences for the detection and localization of local recurrence.

Our study has several limitations. We did not have access to salvage prostatectomy specimens as a reference standard. However, we were able to fully sample the prostate with TPM biopsy. Although no biopsy is free from sampling error,[26] TPM addresses much of the systematic error that is inherent to the transrectal ultrasound-guided biopsy.[27]

mp-MRI was performed using pelvic phased array only without the use of endorectal coil. Although endorectal coil is known to increase the signal-to-noise ratio and potentially increase the sensitivity of T2-weighted imaging,[7,28,29] however, to our knowledge no study has compared endorectal coil with pelvic phased array in the postradiotherapy setting.

Our retrospectively gathered patient cohort incorporates an unavoidable spectrum bias as in other similar studies;[13] patients without a suspicious lesion clinically reported on prebiopsy mp-MRI often opted to avoid TPM and therefore would not have been included within the study cohort. To mitigate the effect of this, we based our analysis at hemigland level, thereby increasing true negative numbers and reducing the disease prevalence (66%) to a level consistent with that reported previously.[9] We believe that the prevalence of disease where mp-MRI is routinely employed for detection of radiorecurrent disease will be lower.

We did not include patients with biochemical failure after brachytherapy[13,15] and therefore our results may not be applicable to this patient population. Brachytherapy seeds can potentially cause image artifact and the effect of this varies with the functional MRI method.[15]

We used more than one mp-MRI platform, 1.5 T and 3 T in our study; however, the impact of that is unknown and has been experienced in other studies.[13] This is in addition to the fact that the value of using higher magnetic resonance strength on performance of MRI has not been clearly recognized.[30]

We did not perform separate locked sequential reads of T2-weighted+DCE imaging or DWI+DCE imaging as we opted to order the sequences based on the potential time/financial cost associated with each additional sequence. Specifically, high *b*-value DWI can be performed faster than the acquisition of data for a full ADC map, and performance of DCE imaging involves additional time and financial cost of the contrast agent. It should be noted, however, that DCE imaging could be beneficial if there is a motion artifact where DWI is difficult to interpret.

## CONCLUSION

Establishing an optimal mp-MRI examination will help reduce examination cost, reduce scan time and improve patient comfort. Although the performance of mp-MRI (T2-weighted+DWI+DCE imaging) was the best, our study shows that a minimum examination of T2-weighted imaging along with high *b*-value DWI acquisition might be all that is necessary for the detection of radiorecurrent prostate cancer. Larger prospective studies are needed to confirm these findings.

## CONFLICT OF INTEREST

The authors declare no conflict of interest.

## ACKNOWLEDGEMENTS

This work was undertaken at the Comprehensive Biomedical Centre, University College Hospital London, which received a proportion of the funding from the National Institute for Health Research. The work was supported by the CRUK/EPSRC KCL/UCL comprehensive cancer imaging centre. The views expressed in this publication are those of the authors and not necessarily those of the UK Department of Health. M Arya acknowledges Orchid (male cancer charity) and Barts and London charity.

## DISCLOSURE

M. Abd-Alazeez receives funding from the Egyptian government. ND was supported by UK EPSRC grants EP/I018700/1 and EP/H046410/1.

## REFERENCES

1 Kara T, Akata D, Akyol F, Karcaaltincaba M, Ozmen M. The value of dynamic contrast-enhanced MRI in the detection of recurrent prostate cancer after external beam radiotherapy: correlation with transrectal ultrasound and pathological findings. *Diagn Interv Radiol* 2011; **17**: 38–43.
2 Roach M 3rd, Hanks G, Thames H Jr., Schellhammer P, Shipley WU, Sokol GH *et al.* Defining biochemical failure following radiotherapy with or without hormonal therapy in men with clinically localized prostate cancer: recommendations of the RTOG-ASTRO Phoenix Consensus Conference. *Int J Radiat Oncol Biol Phys* 2006; **65**: 965–974.
3 Consensus statement: guidelines for PSA following radiation therapy. American Society for Therapeutic Radiology and Oncology Consensus Panel. *Int J Radiat Oncol Biol Phys* 1997; **37**: 1035–1041.
4 Denham JW, Kumar M, Gleeson PS, Lamb DS, Joseph D, Atkinson C *et al.* Recognizing false biochemical failure calls after radiation with or without neoadjuvant androgen deprivation for prostate cancer. *Int J Radiat Oncol Biol Phys* 2009; **74**: 404–411.
5 Pickles T. Prostate-specific antigen (PSA) bounce and other fluctuations: which biochemical relapse definition is least prone to PSA false calls? An analysis of 2030 men treated for prostate cancer with external beam or brachytherapy with or without adjuvant androgen deprivation therapy. *Int J Radiat Oncol Biol Phys* 2006; **64**: 1355–1359.
6 Ornstein DK, Oh J, Herschman JD, Andriole GL. Evaluation and management of the man who has failed primary curative therapy for prostate cancer. *Urol Clin North Am* 1998; **25**: 591–601.
7 Westphalen AC, Kurhanewicz J, Cunha RM, Hsu IC, Kornak J, Zhao S *et al.* T2-weighted endorectal magnetic resonance imaging of prostate cancer after external beam radiation therapy. *Int Braz J Urol* 2009; **35**: 171–180; discussion 181-172.
8 Morgan VA, Riches SF, Giles S, Dearnaley D, deSouza NM. Diffusion-weighted MRI for locally recurrent prostate cancer after external beam radiotherapy. *AJR Am J Roentgenol* 2012; **198**: 596–602.
9 Westphalen AC, Coakley FV, Roach M 3rd, McCulloch CE, Kurhanewicz J. Locally recurrent prostate cancer after external beam radiation therapy: diagnostic performance of 1.5-T endorectal MR imaging and MR spectroscopic imaging for detection. *Radiology* 2010; **256**: 485–492.
10 Kim CK, Park BK, Lee HM. Prediction of locally recurrent prostate cancer after radiation therapy: incremental value of 3T diffusion-weighted MRI. *J Magn Reson Imaging* 2009; **29**: 391–397.
11 Haider MA, Chung P, Sweet J, Toi A, Jhaveri K, Menard C *et al.* Dynamic contrast-enhanced magnetic resonance imaging for localization of recurrent prostate cancer after external beam radiotherapy. *Int J Radiat Oncol Biol Phys* 2008; **70**: 425–430.
12 Westphalen AC, Reed GD, Vinh PP, Sotto C, Vigneron DB, Kurhanewicz J. Multiparametric 3T endorectal MRI after external beam radiation therapy for prostate cancer. *J Magn Reson Imaging* 2012; **36**: 430–437.
13 Akin O, Gultekin DH, Vargas HA, Zheng J, Moskowitz C, Pei X *et al.* Incremental value of diffusion weighted and dynamic contrast enhanced MRI in the detection of locally recurrent prostate cancer after radiation treatment: preliminary results. *Eur Radiol* 2011; **21**: 1970–1978.
14 Arumainayagam N, Ahmed HU, Moore CM, Freeman A, Allen C, Sohaib SA *et al.* Multiparametric MR imaging for detection of clinically significant prostate cancer: a validation cohort study with transperineal template prostate mapping as the reference standard. *Radiology* 2013; **268**: 761–769.

15 Donati OF, Jung SI, Vargas HA, Gultekin DH, Zheng J, Moskowitz CS *et al.* Multiparametric prostate MR imaging with T2-weighted, diffusion-weighted, and dynamic contrast-enhanced sequences: are all pulse sequences necessary to detect locally recurrent prostate cancer after radiation therapy? *Radiology* 2013; **268**: 440–450.
16 Kumbhani SR, Coakley FV, McCulloch CE, Wang ZJ, Kurhanewicz J, Roach M 3rd *et al.* Endorectal MRI after radiation therapy: questioning the sextant analysis. *J Magn Reson Imaging* 2011; **33**: 1086–1090.
17 Kim CK, Park BK, Park W, Kim SS. Prostate MR imaging at 3T using a phased-arrayed coil in predicting locally recurrent prostate cancer after radiation therapy: preliminary experience. *Abdom Imaging* 2010; **35**: 246–252.
18 Arumainayagam N, Kumaar S, Ahmed HU, Moore CM, Payne H, Freeman A *et al.* Accuracy of multiparametric magnetic resonance imaging in detecting recurrent prostate cancer after radiotherapy. *BJU Int* 2010; **106**: 991–997.
19 Tamada T, Sone T, Jo Y, Hiratsuka J, Higaki A, Higashi H *et al.* Locally recurrent prostate cancer after high-dose-rate brachytherapy: the value of diffusion-weighted imaging, dynamic contrast-enhanced MRI, and T2-weighted imaging in localizing tumors. *AJR Am J Roentgenol* 2011; **197**: 408–414.
20 Barentsz JO, Richenberg J, Clements R, Choyke P, Verma S, Villeirs G *et al.* ESUR prostate MR guidelines 2012. *Eur Radiol* 2012; **22**: 746–757.
21 Barzell WE, Melamed MR. Appropriate patient selection in the focal treatment of prostate cancer: the role of transperineal 3-dimensional pathologic mapping of the prostate--a 4-year experience. *Urology* 2007; **70**: 27–35.
22 Karram S, Trock BJ, Netto GJ, Epstein JI. Should intervening benign tissue be included in the measurement of discontinuous foci of cancer on prostate needle biopsy? Correlation with radical prostatectomy findings. *Am J Surg Pathol* 2011; **35**: 1351–1355.
23 Hanley JA, McNeil BJ. The meaning and use of the area under a receiver operating characteristic (ROC) curve. *Radiology* 1982; **143**: 29–36.
24 Landis JR, Koch GG. The measurement of observer agreement for categorical data. *Biometrics* 1977; **33**: 159–174.
25 Rud E, Baco E, Lien D, Klotz D, Eggesbo HB. Detection of radiorecurrent prostate cancer using diffusion-weighted imaging and targeted biopsies. *AJR Am J Roentgenol* 2014; **202**: W241–W246.
26 Robertson NL, Hu Y, Ahmed HU, Freeman A, Barratt D, Emberton M. Prostate Cancer Risk Inflation as a Consequence of Image-targeted Biopsy of the Prostate: A Computer Simulation Study. *Eur Urol* 2013; **65**: 628–634.
27 Hu Y, Ahmed HU, Carter T, Arumainayagam N, Lecornet E, Barzell W *et al.* A biopsy simulation study to assess the accuracy of several transrectal ultrasonography (TRUS)-biopsy strategies compared with template prostate mapping biopsies in patients who have undergone radical prostatectomy. *BJU Int* 2012; **110**: 812–820.
28 Heijmink SW, Futterer JJ, Hambrock T, Takahashi S, Scheenen TW, Huisman HJ *et al.* Prostate cancer: body-array versus endorectal coil MR imaging at 3T--comparison of image quality, localization, and staging performance. *Radiology* 2007; **244**: 184–195.
29 Sala E, Eberhardt SC, Akin O, Moskowitz CS, Onyebuchi CN, Kuroiwa K *et al.* Endorectal MR imaging before salvage prostatectomy: tumor localization and staging. *Radiology* 2006; **238**: 176–183.
30 Park BK, Kim B, Kim CK, Lee HM, Kwon GY. Comparison of phased-array 3.0-T and endorectal 1.5-T magnetic resonance imaging in the evaluation of local staging accuracy for prostate cancer. *J Comput Assist Tomogr* 2007; **31**: 534–538.
31 Ahmed HU, Hu Y, Carter T, Arumainayagam N, Lecornet E, Freeman A *et al.* Characterizing clinically significant prostate cancer using template prostate mapping biopsy. *J Urol* 2011; **186**: 458.
32 Abd-Alazeez M, Kirkham A, Ahmed HU, Arya M, Anastasiadis E, Charman SC *et al.* Performance of multiparametric MRI in men at risk of prostate cancer before the first biopsy: a paired validating cohort study using template prostate mapping biopsies as the reference standard. *Prostate Cancer Prostatic Dis* 2014; **17**: 40.
33 Abd-Alazeez M, Ahmed HU, Arya M, Charman SC, Anastasiadis E, Freeman A *et al.* The accuracy of multiparametric MRI in men with negative biopsy and elevated PSA level—can it rule out clinically significant prostate cancer?. *Urol Oncol* 2014; **32**: 45.e17.

## APPENDIX

The appendix presents a sub-analysis of the data based on a definition of clinical significance of prostate cancer. Clinically significant disease was defined as either a lesion of Gleason 3+4 and/or lesion size $>0.2\,cm^3$.[31] We have previously used this definition for the classification of clinically significant disease at diagnosis.[32,33]

Within the appendix we evaluate the presence of clinically significant tumor based on two separate mp-MRI score thresholds (3 and 4).

Significant prostate cancer was present in 32/37 (86%) men and 46/74 (62%) hemiglands.

**Table 1A.** Patient demographics

| | *All patients* (n = *37*) | *Patients without significant cancer* (n = *5*) | *Patients with significant cancer* (n = *32*) |
|---|---|---|---|
| Age | 68 (57–80) | 69 (62–79) | 68 (57–80) |
| PSA at time of MRI | 4.5 (0.5–60) | 2.4 (0.5–5.8) | 4.75 (0.6–60) |
| Time between end of DXT and MRI (months) | 66 (24–166) | 57 (54–72) | 66.5 (24–166) |
| Time between MRI and biopsy (months) | 2 (1–10) | 2 (1–10) | 1.5 (1–6) |
| Total biopsy cores/patient | 41 (20–85) | 33 (22–41) | 45 (20–85) |
| Positive cores/patient (%) | 17 (0–96) | 0 (0–3) | 20.5 (6–96) |
| *Clinical stage at diagnosis* | | | |
| 1b | 1 | 0 | 1 |
| 1c | 8 | 1 | 7 |
| 2a | 7 | 3 | 4 |
| 2b | 1 | 1 | 0 |
| 2c | 4 | 0 | 4 |
| 3a | 10 | 0 | 10 |
| 3b | 6 | 0 | 6 |
| *Gleason score at diagnosis* | | | |
| 3+3 | 15 | 2 | 13 |
| 3+4 | 9 | 1 | 8 |
| 4+3 | 2 | 0 | 2 |
| 4+4 | 4 | 1 | 3 |
| 4+5 | 6 | 1 | 5 |
| 5+4 | 1 | 0 | 1 |
| *Hormones before MRI* | | | |
| Yes | 27 | 4 | 23 |
| No | 10 | 1 | 9 |

Abbreviation: DXT, deep x-ray therapy; MRI, magnetic resonance imaging.

**Table 2A.** Reader performance at the hemigland level with mp-MRI score >3 as positive

| | *R1* | | | | *R2* | | | |
|---|---|---|---|---|---|---|---|---|
| | *T2W* | *T2W+high* b-*value* | *T2W+high* b-*value +ADC* | *T2W+high* b-*value+ADC +DCE* | *T2W* | *T2W+high* b-*value* | *T2W+high* b-*value +ADC* | *T2W+high* b-*value+ADC +DCE* |
| Sensitivity | 76 | 74 | 67 | 85 | 80 | 70 | 67 | 80 |
| Specificity | 50 | 89 | 89 | 71 | 46 | 93 | 93 | 75 |
| Positive PV | 71 | 92 | 91 | 83 | 71 | 94 | 94 | 84 |
| Negative PV | 56 | 68 | 63 | 74 | 59 | 65 | 63 | 70 |

Abbreviations: ADC, apparent diffusion coefficient; DCE, dynamic contrast-enhanced imaging; mp-MRI, multiparametric magnetic resonance imaging; PV, predictive value; R1, reader 1; R2, reader 2; T2W, T2 weighted.

**Table 3A.** Reader performance at the hemigland level with mp-MRI score >4 as positive

| | *R1* | | | | *R2* | | | |
|---|---|---|---|---|---|---|---|---|
| | *T2W* | *T2W+high* b-*value* | *T2W+high* b-*value +ADC* | *T2W+high* b-*value+ADC +DCE* | *T2W* | *T2W+high* b-*value* | *T2W+high* b-*value+ ADC* | *T2W+high* b-*value+ADC+ DCE* |
| Sensitivity | 15 | 43 | 43 | 67 | 26 | 50 | 46 | 74 |
| Specificity | 100 | 96 | 96 | 93 | 100 | 100 | 100 | 93 |
| Positive PV | 100 | 95 | 95 | 94 | 100 | 100 | 100 | 94 |
| Negative PV | 42 | 51 | 51 | 63 | 45 | 55 | 53 | 68 |

Abbreviations: ADC, apparent diffusion coefficient; DCE, dynamic contrast-enhanced imaging; mp-MRI, multiparametric magnetic resonance imaging; PV, predictive value; R1, reader 1; R2, reader 2; T2W, T2 weighted.